Energy 141 (2017) 1928–1939

Contents lists available at ScienceDirect

Energy

journal homepage: www.elsevier.com/locate/energy

Experimental and theoretical investigation of a flat heat pipe heat exchanger for waste heat recovery in the steel industry

Hussam Jouhara [a, *], Sulaiman Almahmoud [a], Amisha Chauhan [a], Bertrand Delpech [a], Giuseppe Bianchi [a], Savvas A. Tassou [a], Rocio Llera [b], Francisco Lago [b], Juan José Arribas [b]

[a] Institute of Energy Futures, College of Engineering, Design and Physical Sciences, Brunel University London, UB8 3PH, UK
[b] ArcelorMittal Global R&D Asturias, P.O. Box 90, Avilés 33400, Spain

ARTICLE INFO

Article history:
Received 26 July 2017
Received in revised form
25 October 2017
Accepted 31 October 2017
Available online 30 November 2017

Keywords:
Flat heat pipe
Heat exchanger
Waste heat recovery

ABSTRACT

Most of the energy demand in the steel industry is used for heating purposes. The recovery of residual heat contributes to significant reductions in both production costs and greenhouse gas emissions. In this paper, the design, manufacture and testing of an innovative heat recovery system based on a Flat Heat Pipe heat exchanger (FHP) is described. The FHP system consists of stainless steel heat pipes linked by a bottom header and a shell and tube top header. The thermal performance of the FHP was investigated both in the laboratory and on an industrial plant and the energy recovered and the working temperatures of the FHP are reported. A theoretical modelling tool has been built to predict the performance of the device in the laboratory. Reasonable agreement has been obtained between experimental and theoretical results. It is concluded from the results that the FHP is an innovative high efficiency technology for waste heat recovery from such industrial applications.

1. Introduction

The steel industry is one of the largest energy-consuming industries, accounting for 5% of the total world energy consumption with energy costs representing about 30% of total production costs. Heat recovery from the steel manufacturing process is a huge challenge due to many difficulties such as the space available for installing heat exchangers and matching the waste heat stream to the heat sink demand. Recovering excess heat from the processes could reduce greenhouse gas emissions and significantly reduce production costs. A significant number of investigations on waste heat recovery have been conducted over the past decade. The majority of innovations have focused on molten slag heat recovery as discussed by *Zhang* et al. [1], *Liu* et al. [2], and *Gutiérrez-Trashorras* et al. [3]. Four waste heat recovery systems have been investigated: Air blast, Single Drum, Twins Drums, and the Spinning Cup methods; typically these systems have an average efficiency of approximately 50%. *Kaşka* [4] proposed an Organic Rankine Cycle for power generation using the excess heat of a walking beam slab reheat furnace. The system proposed was tested with different working fluids for two working conditions. The first case was with a gross power production of 260 kW. The second case was with a gross power production of 200 kW. The ORC designed had energy and exergy efficiencies of 10.2%, 48.5% and 8.8%, 42.2%, respectively, for the two cases.

Most of those technologies are not able to recover enough waste heat to be a viable solution for companies. However utilising heat pipe based heat exchangers for waste heat recovery is a promising solution that can address this issue. Heat pipe technology is recognized as a high efficiency transfer method. Where heat pipes are passive thermal devices that are able to transfer large amount of heat with no moving parts, using only the phase change (liquid-vapour) process. The heat pipe is composed of a shell case material and a working fluid. The system is separated in three sections, the evaporator section where heat is applied; the adiabatic section composed of liquid and vapour; and the condenser section where the vapour is condensing. Fig. 1 illustrates the heat pipe concept.

When heat is applied on the evaporator section, the working fluid vaporizes. The vapour then travels through the adiabatic section to the condenser. The latent heat of the vapour is then transferred to the condenser surrounding which causes the condensation of the working fluid. The working fluid then flows back to the evaporator. The working fluid can be transported to the

* Corresponding author.
E-mail address: hussam.jouhara@brunel.ac.uk (H. Jouhara).

https://doi.org/10.1016/j.energy.2017.10.142

Nomenclature

Symbol

A	Surface area (m^2)
C_p	Specific heat (J/kg.K)
C_{sf}	constant, determined from experimental data
D	Diameter (m)
$F_{eo,h}$	View factor
g	Gravitational acceleration (m/s^2)
h	Heat transfer Coefficient (W/m^2. K)
h_{fg}	Latent heat of vaporization (J/kg)
k	Thermal conductivity of liquid (W/m. K)
l	Length (m)
$\dot{m}$	mass flow rate (kg/s)
N	number of pipes
Nu	Nusselt number
Pr	Prandtl number
p_r	Reduced pressure
Q	Heat transfer rate (W)
R	Thermal resistance (°C/W)
Re	Reynolds number
T	Temperature (K)

Greek Symbols

α	liquid thermal diffusivity (m^2/s)
μ	Dynamic viscosity (kg/m.s)
ρ	Density (kg/m^3)
σ	Surface tension (N/m)
σ_0	Stefan–Boltzmann constant which is equal to 5.67×10^{-8} $W/(m^2. K^4)$
ε	Radiation emissivity

Subscripts

c	Condenser section
ci	Corresponds to inner wall of condenser
co	Corresponds to outer wall of condenser
$cold, in$	Cooling fluid inlet
$cold, out$	Cooling fluid outlet
$Cond, e$	Evaporator wall conduction
$Cond, c$	Condenser wall conduction
ei	Corresponds to inner wall of evaporator
eo	Corresponds to outer wall of evaporator
f	Factor for heat transfer in forced convection
h	Heat source
l	Liquid
rad	radiation
v	Vapour

Superscripts

n	experimental constant that depends on fluid

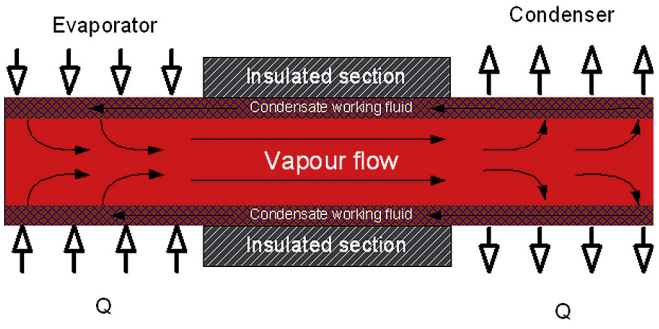

Fig. 1. Pipe working cycle [5].

evaporator using wick or by gravity [6–10].

Heat pipe technology has been investigated for many different applications such as waste heat recovery [11,12] and solar applications [13–18]. *Tian* et al. [19] investigated a new type of heat pipe based heat exchanger for waste heat recovery from flue gases. The heat pipe consists of a condensing shell and tube chamber and a finned pipe evaporator. Clean air was used to pre-heat the burner air supply, leading to a reduction of 15% in natural gas consumption and therefore a reduction in greenhouse gas emissions. *Azad* [20] presented a design of wicked heat pipe for a solar collector. The design configuration consisted of six vertical copper tubes connected by a horizontal tube at the bottom end and a header at the top end. The investigation of the heat pipe, the collector, and cooling fluid temperatures in addition to the collector efficiency showed agreement between theoretical and experimental results. The analytical model developed was validated by comparing the theoretical results with the experimental outcomes in literature [21].

Heat pipes generally are cylindrical pipes, however the evaporator or condenser or both can be flat. In this case it is called a flat heat pipe. The advantages of flat heat pipe technology are the isothermal characteristics and flat evaporator surface which maximises the radiation absorbing area [22].

Flat heat pipes are commonly used in heat dissipation of electrical and electronic devices as they are able to transport high heat flux and make thermal management of such devices feasible. A substantial amount of research was conducted on flat heat pipes and vapour chambers [23,24]. The main focus of the investigation was based on the effect of the heat transfer rate on the thermal resistance of the heat pipe and the isothermal characteristics of the heat pipe [25–33].

Flat heat pipes can also utilised in solar applications when combined with PV panels [34]. Joining heat pipes with PV panels makes the system produce electricity and thermal heat simultaneously. This combination of flat heat pipe with PV panels increases the efficiency of PV panel by decreasing the working temperature of the panel [35].

Jouhara et al. [36] developed and validated a novel flat heat pipe based photovoltaic thermal (PV/T) system called a 'heat mat', where the new design performs as a building envelope. The experiments examined the effects of cooling cycles on the electrical output and the temperature of the heat pipe PV/T panels. The electrical efficiency was increased by 15% with the use of an active cooling cycle in the panels. Moreover, the temperature of the panels decreased from the range of 40 °C–58 °C to the range of 28 °C–33 °C. The thermal efficiency of the heat mat without the PV layer was around 64%, while the efficiency of the heat mat with the PV layer was around 50%. The ability of the heat mat to absorb heat from the ambient was also studied as a function of air speed and the temperature difference between the ambient and cooling water.

Heat pipes with flat evaporators are also used in solar thermochemical reactors which are considered a special case of solar receivers, where solar energy is utilised in chemical reactions in the

reactor to produce solar fuel. A heat pipe design which combined a flat evaporator and a cylindrical condenser was proposed and investigated by *Wang* et al. [37]. The heat pipe showed a uniform thermal distribution on the condenser and evaporator sections. *Yang* et al. [38] proposed a design of a high temperature flat heat pipe receiver in a solar power tower plant. The start-up and the thermal performance of the system were experimentally investigated. The impact of inclination angle and heat input on the start-up time and temperature distribution were tested and the best performance was obtained at an angle of 45°. The effective thermal conductivity, thermal resistance, and heat transfer efficiency of the FHP were calculated at various inputs. It was noted that the thermal resistance decreases as the heat input increases, whilst the efficiency is enhanced as the heat input increases. The stability in operation was also studied and the FHP exhibited the potential of long term, safe and uniform temperature distributions.

In this paper a flat heat pipe is described, which is designed to recover heat transferred by radiation and convection from sources such as hot metal in the steel industry at temperatures higher than 500 °C. The design of the FHP is presented and the results for experimental investigations reported. A theoretical model has been developed to predict the performance of the flat heat pipe and experimental and theoretical results are compared.

2. Mechanical design of the flat heat pipe heat exchanger

The Flat Heat Pipe is designed to recover heat mainly by thermal radiation from sources at temperatures greater than 500 °C. The radiation is absorbed by the outer surface of the FHP and transferred by conduction through the heat pipe evaporator wall to the inner surface. When the working fluid reaches the saturation temperature, it vaporizes and flows upwards to the condenser. The heat is then transferred to the cooling fluid via a shell and tube heat exchanger system, which condenses the working fluid. Finally, the condensate flows back to the evaporator section under gravity.

The prototype of the flat heat pipe illustrated in Fig. 2 (a) consists of 14 stainless steel pipes with a length of 1 m linked by a bottom header and a shell and tube heat exchanger at the top. The shell and tube heat exchanger consists of 8 stainless steel smooth tubes within a stainless steel shell. A stainless steel sheet is fixed at the back of the evaporator section to increase the overall heat transfer area. The overall dimensions of the flat heat pipe are 1 m height by 1 m width. A stand has been designed and manufactured to hold the system in place as shown in Fig. 2 (b). This allows the system to be tested at different inclinations and heights.

3. Experimental arrangements

3.1. Laboratory tests

The FHP was tested in a laboratory in order to validate the thermal design and the theoretical prediction for the heat transfer rate. The test rig is shown in Fig. 3 (a). The FHP was installed in front of electrical heaters to capture the radiative heat from the hot source. The FHP was charged with water and installed at an initial inclination angle of 12.5° receiving the heat from the bottom plate. The top plate heaters were not used during this test. The back panel, the adiabatic section, and the water pipes were insulated to prevent heat losses to the ambient as shown in Fig. 3 (b).

Temperatures were measured using K type thermocouples, where the uncertainties associated with the temperature readings are (0.05% rdg + 0.3 °C). The flow rate was measured using a flow meter (Omega FTB 371 turbine flow sensor where the uncertainty associated with the readings is ±1% full scale). This instrumentation was connected to a data logging system. The thermocouple positions are shown in Fig. 3. Three thermocouples were installed on the bottom header (EV 1–3), an additional five on the vertical heat pipes to measure the surface temperature (HP 1–5), three on the adiabatic section to measure the saturation temperature of the working fluid (AD 1–3), one on the back panel of the FHP (BP), and two thermocouples measured water inlet and outlet temperatures. High temperature thermal insulation was used to insulate the condenser of the FHP and the back panel to minimize heat losses to the surroundings. The water supply pipe was also insulated to avoid any radiative heat transfer to the water.

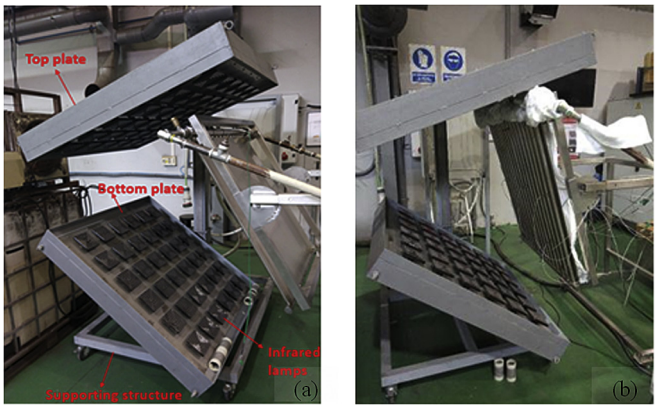

Fig. 3. Experimental apparatus of the FHP: (a) FHP positioning, (b) FHP test setup after the insulation.

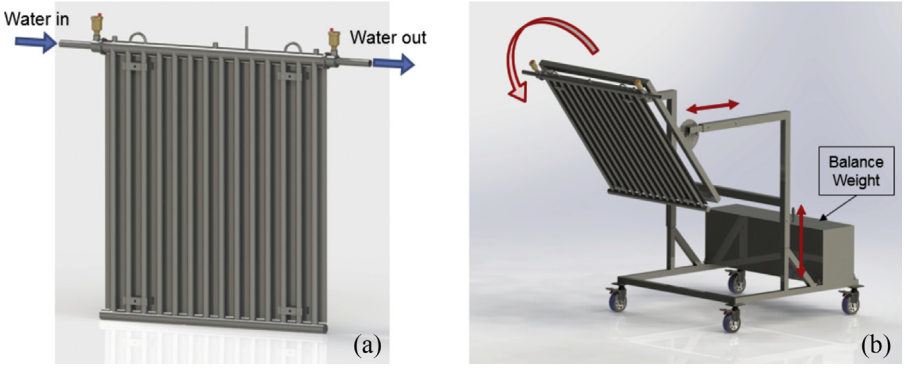

Fig. 2. The mechanical design of the FHP: (a) FHP design, (b) FHP stand.

Table 1
Experimental conditions (Laboratory tests).

Test#	1	2
Heater temperature	500 °C	580 °C
Heater power	25 kW	29 kW
FHP inclination angle from the vertical	12.5°	
Water flow rate	25 L/min = 0.42 kg/s	
Water inlet temperature	10.6 °C	

Two tests were conducted at the same water flow rate. Test 1 was performed at a heater temperature of 500 °C, which was measured by a laser pyrometer, while test 2 was performed at a heater temperature of 580 °C. The experimental conditions are summarised in Table 1 Experimental conditions (Laboratory tests).

3.2. Industrial tests

The flat heat pipe was tested on a production line during the cooling process of steel wires. The total length of the production line was 70 m. The FHP was placed 5.75 m from the beginning of the production line, at the hottest point of the cooling zone. Temperatures were again measured using K type thermocouples; although for these tests the number of thermocouples on the heat pipes was increased from five to nine, see Figs. 4 and 5. The speed and temperature of the air used to cool the wire was measured using a Testo 425 portable anemometer. The Flat Heat Pipe was installed with an initial inclination angle of 12.5° to the vertical. High temperature thermal insulation was used to insulate the top header of the FHP and the back panel to minimize heat loss to the surroundings. The water supply pipe was also insulated to minimize radiant heat transfer to the incoming water. The on-site test of the FHP is shown in Fig. 6.

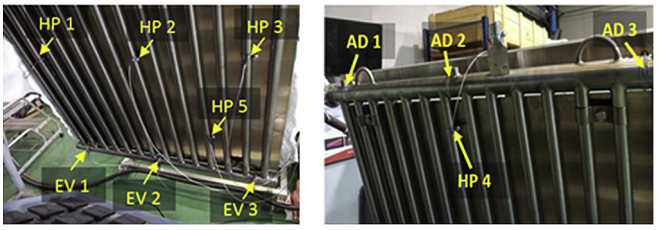

Fig. 4. Thermocouples positions.

The experimental conditions including FHP positioning and water parameters are presented in Table 2.

The concept of testing the Flat heat pipe is illustrated in Fig. 7 (a) and (b) (see Table 3). Fig. 7 (a) shows the FHP positioning in test 1 where the distance between the FHP and the edge of the barrier 65 cm while in test 2 the FHP was placed above the steel wires with a distance of 6 cm from the barrier edge from the inner side, which is illustrated in Fig. 7 (b).

4. Theoretical investigation

A modelling tool was built in Visual Basic to predict the thermal performance of the FHP. As mentioned in paragraph 2, the Flat Heat Pipe is considered as a thermosiphon. In order to predict the performance of the flat heat pipe, thermal network analogy method is used. The thermal network of the Flat Heat Pipe is presented in Fig. 8.

The thermal resistances can be treated as electrical resistances.where:

R_{rad}: Radiation thermal resistance of evaporator section.
R_{cond_e}: Conduction thermal resistance of the evaporator wall
R_{ei}: Boiling thermal resistance
R_{ci}: Condensation Thermal resistance
R_{cond_c}: Conduction thermal resistance of the condenser wall
R_{co}: Convection thermal resistance of condenser section

The heat pipe resistance and heat transfer rate through the heat pipe, respectively can be calculated as follows:

$$R_{hp} = R_{cond\_e} + R_{ei} + R_{co} + R_{cond\_c} \quad (1)$$

$$Q_{hp} = \frac{T_{eo} - T_{ci}}{R_{hp}} \quad (2)$$

4.1. Radiation

Thermal resistance of radiation can be calculated according to the approach explained in Ref. [39] as shown in Fig. 9. Where the radiative heat is transferred from the hot steel that has the temperature T_h to the outer surface of the evaporator of the flat heat pipe which has the temperature,T_{eo} [40].

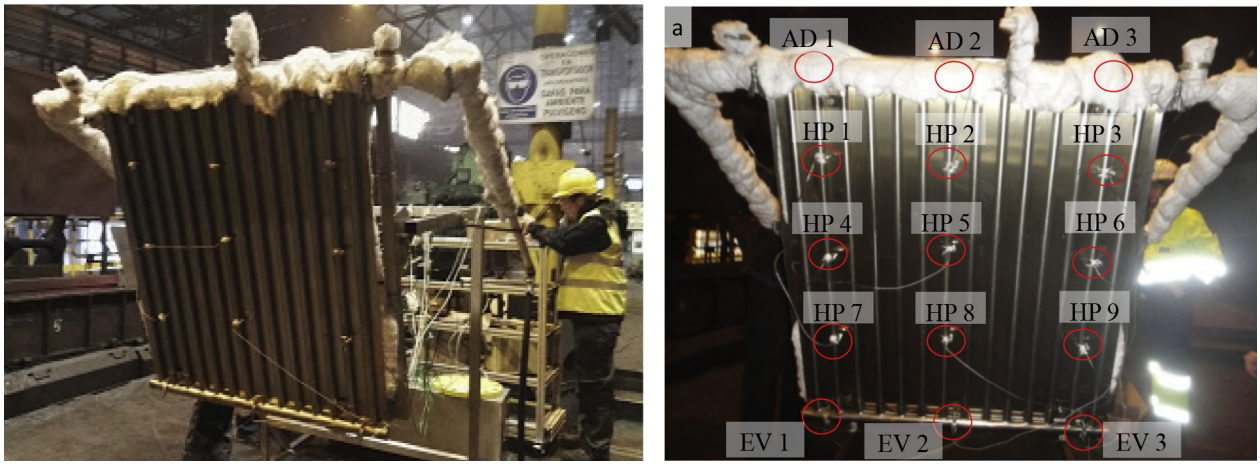

Fig. 5. Industrial set up and Thermocouple positions.

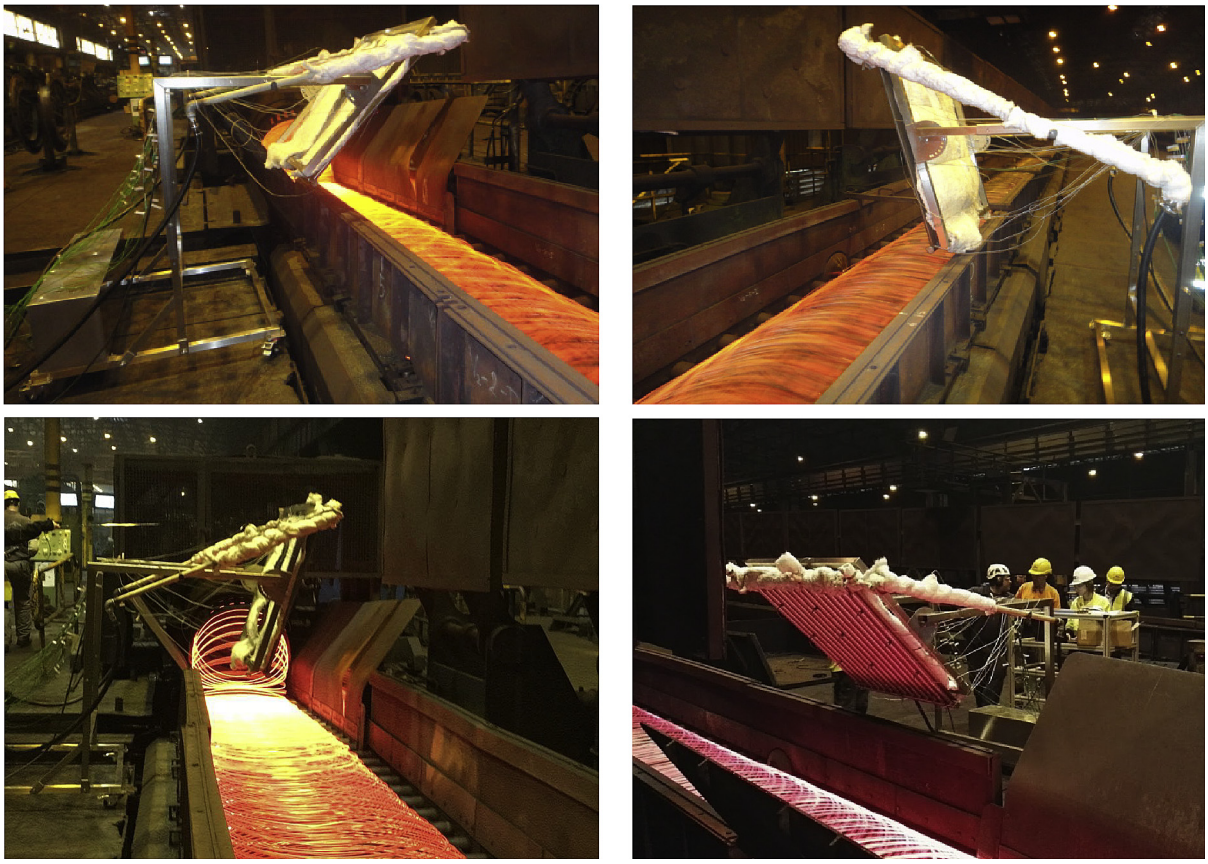

Fig. 6. FHP Industrial testing.

Table 2
Experimental conditions (Industrial tests).

Test#	1	2
Air temperature above the hot wires	136 °C	
Air cooling velocity	6.75 m/s	12 m/s
Wire temperature	450 °C	450 °C
Distance between the FHP and the edge of the barrier	65 cm	6 cm
Distance between the FHP and the beginning of the production line	575 cm	
FHP inclination angle from the vertical	12.5°	
Water flow rate	25 L/min = 0.42 kg/s	
Water inlet	26.2 °C	34.7 °C

$$Q_{rad} = \frac{\sigma_0\left(T_h^4 - T_{eo}^4\right)}{\frac{1-\varepsilon_{eo}}{\varepsilon_{eo}A_{eo}} + \frac{1}{A_{eo}F_{eo,\ h}} + \frac{1-\varepsilon_h}{A_h\varepsilon_h}} = \frac{T_h - T_{eo}}{R_{rad}} \quad (3)$$

$$R_{rad} = \frac{\frac{1-\varepsilon_{eo}}{\varepsilon_{eo}A_{eo}} + \frac{1}{A_{eo}F_{eo,\ h}} + \frac{1-\varepsilon_h}{A_h\varepsilon_h}}{\sigma_0\left(T_h^2 + T_{eo}^2\right)(T_h + T_{eo})} \quad (4)$$

$$A_{eo} = \frac{\pi}{2} \times D_{eo} \times L_e \times N_{evaporator\ pipes} + \eta A_{sheet} \quad (5)$$

where.

ε_{eo}: is the radiation emissivity of the evaporator wall surface
ε_h: is the radiation emissivity of the heat source

$F_{eo,\ h}$: A view factor its value is between 0 and 1 depending on the orientation of the flat heat pipe and the heat source in addition to the shape of the flat heat pipe.
T_h : Temperature of the heat source in (K)
T_{eo}: Temperature of outer wall of the evaporator (K)
σ_0: Stefan–Boltzmann constant which is equal to 5.67×10^{-8}W/(m$^2\cdot$K^4)

For boiling Resistance:

$$R_{ei} = \frac{1}{h_{ei}\cdot A_{ei}} \quad (6)$$

A_{ei}: heat pipe evaporator inner area (m^2)

$$A_{ei} = \frac{\pi}{2} \times D_{ei} \times L_e \times N_{evaporator\ pipes} \quad (7)$$

D_{ei}: Evaporator inner diameter
L_e: Evaporator length
h_{ei}: Boiling heat transfer coefficient (W/m^2. °C)

The boiling heat transfer coefficient can be calculated from Roshenow [41] correlation:

$$h_{ei} = \mu_l\cdot h_{fg}\left[\frac{g\cdot(\rho_l - \rho_v)}{\sigma}\right]^{\frac{1}{2}}\cdot\left[\frac{c_p}{\left(C_{sf}\cdot h_{fg}\cdot Pr_l^n\right)}\right]^3\cdot(T_{ei} - T_v)^2 \quad (8)$$

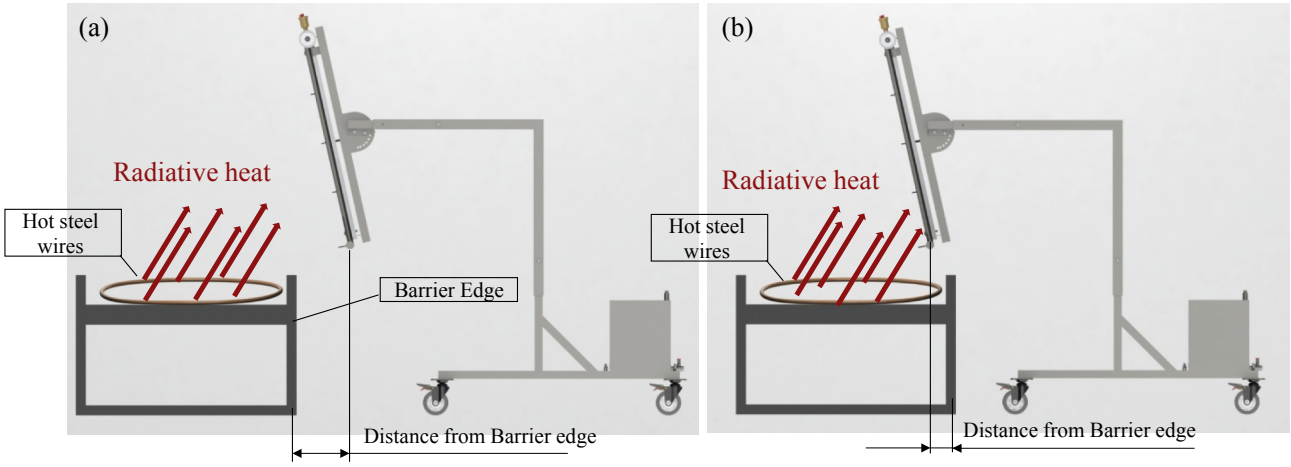

Fig. 7. 3D drawing of the flat heat pipe positioning during the factory tests: (a) Test 1, (b) Test 2.

Table 3
Experimental uncertainty.

Test	Maximum Heat transfer rate (kW)	Error: S_Q (kW)	Error (%)
Test 1 Laboratory	11.4	0.768	±6.77%
Test 2 Laboratory	11.5	0.768	±6.7%
Test 1 Factory	16.9	0.762	±4.51%
Test 2 Factory	16.1	0.8	±4.97%

And the heat transfer rate by boiling can be calculated by the following equation

$$Q_{ei} = \frac{(T_{ei} - T_v)}{R_{ei}} \quad (9)$$

The heat pipe condenser resistance is given as follows:

$$R_{co} = \frac{1}{h_{co} \cdot A_{co}} \quad (10)$$

A_{co}: Heat pipe condenser area (m^2). Where:

$$A_{co} = A_{water\ pipe} \times N_{waterpipes} \quad (11)$$

$$A_{co} = \pi \times D_{co} \times L_c \times N_{water\ pipes} \quad (12)$$

D_{co}: Condenser outer diameter
L_c: Condenser length

The condensation heat transfer coefficient can be calculated by using Nusselt [42] correlation:

$$h_{ci} = 0.725 \left[\frac{\rho_l(\rho_l - \rho_v) g h_{fg}^* k_l^3}{D_{co} \mu_l (T_v - T_{co})} \right]^{\frac{1}{4}} \quad (13)$$

where h_{fg}^* is the modified latent heat of vaporization which is calculated by the following formula [43]:

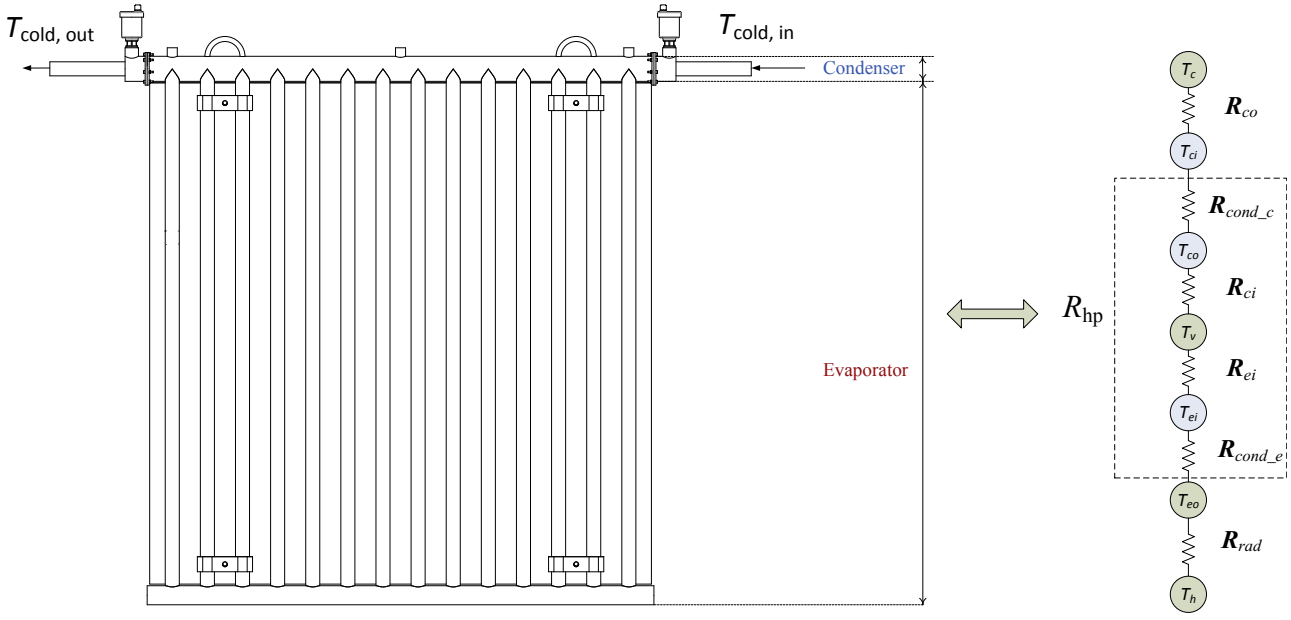

Fig. 8. Schematic of the thermal resistances within the flat heat pipe.

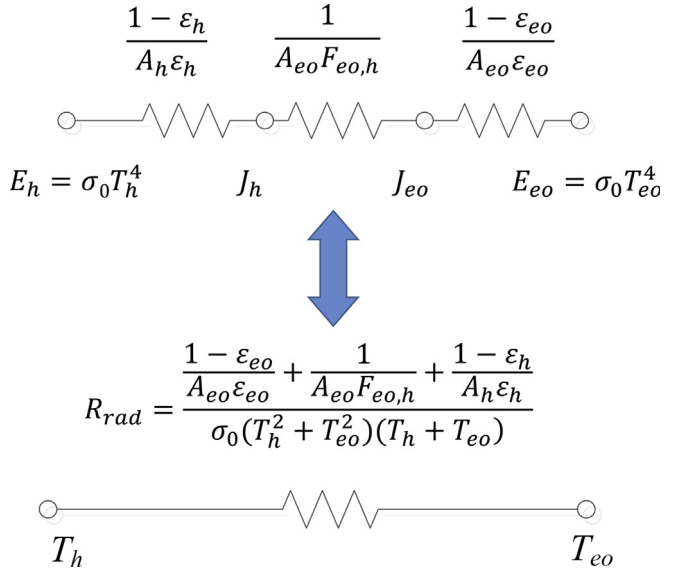

Fig. 9. Radiation heat resistance.

$$h_{fg}^{*} = h_{fg} + 0.68C_p(T_v - T_{co}) \tag{14}$$

The heat transfer rate by condensation is calculated by the following equation:

$$Q_{co} = \frac{(T_v - T_{co})}{R_{co}} \tag{15}$$

The forced convection resistance is given as follows:

$$R_{ci} = \frac{1}{h_{ci}\cdot A_{ci}} \tag{16}$$

$$A_{ci} = \pi \times D_{ci} \times L_c \times N_{water\ pipes} \tag{17}$$

where:

D_{ci}: Condenser inner diameter
L_c: Condenser length
h_{ci}: Forced convection heat transfer coefficient

The forced convection heat transfer coefficient is calculated by using Gnielinski [44] correlation:

$$Nu = \frac{(f/8)(Re - 1000)Pr}{1 + 12.7(f/8)^{1/2}(\mathrm{Pr}^{2/3} - 1)}\left[1 + (D_{ci}/L_c)^{2/3}\right]\left(\frac{Pr}{Pr_{ci}}\right)^{0.11} \tag{18}$$

This correlation is applicable for the Reynolds number in the range of. $2300 < Re < 5 \times 10^6$Where f is a factor calculated from the following correlation:

$$f = (1.82\log_{10}Re - 1.64)^{-2} \tag{19}$$

The heat transfer rate by forced convection is calculated by the following:

$$Q_{co} = h_{ci}\cdot A_{ci}\cdot LMTD = \frac{LMTD}{R_{ci}} \tag{20}$$

Where *LMTD* is the logarithmic mean temperature of the cooling fluid

$$LMTD = \left(\frac{(T_{ci} - T_{cold,\ in}) - (T_{ci} - T_{cold,out})}{\ln\left(\frac{T_{ci}-T_{cold,out}}{T_{ci}-T_{cold,\ in}}\right)}\right) \tag{21}$$

Conduction resistances are given as follows: The thermal resistance of evaporator wall conductivity is given as follow:

$$R_{conde\_e} = \frac{\ln(D_{eo}/D_{ei})}{\pi L_e k_s N_{evaporator\ pipes}} \tag{22}$$

In similar way, the thermal resistance of wall conductivity of the condenser is given as follow:

$$R_{conde\_c} = \frac{\ln(D_{co}/D_{ci})}{2\pi L_c k_s N_{water\ pipes}} \tag{23}$$

In the theoretical calculation of heat transfer through the evaporator, the heat transfer area was considered to be half of the total evaporator area since the evaporator is insulated from the back.

The heat transfer rate in the condenser section can be calculated from the following equation also:

$$Q_{co} = \dot{m}\cdot C_p\cdot(T_{cold,out} - T_{cold,in}) \tag{24}$$

5. Results and discussion

5.1. Laboratory tests

The temperatures of the FHP surface in test 1 and test 2 are presented in Fig. 10. The surface temperature of the FHP during test 1 varied between 63.5 °C and 80.3 °C. It was observed that the temperature of thermocouple HP 4 was the highest due to is position which reflected a maximum temperature of 80.3 °C during test 1. The surface temperatures of the flat heat pipe varied between 64.4 °C and 85.4 °C in test 2. It can be observed from the results that the temperatures of the thermocouples HP 1–3 were nearly the same. Thermocouple HP 5 had the lowest temperature value. This temperature could be explained by a false junction along the thermocouple or an incorrect installation. The back panel temperature was 102.7 °C and 92 °C in test 1 and test 2, respectively. The back panel temperature was higher than the pipe temperatures since the thermal conductivity of the stainless steel sheet is relatively low.

The temperature of the bottom header and the adiabatic section of the FHP, plus water inlet and outlet temperatures are illustrated in Fig. 11 for both tests. In test 1 the average temperature of the bottom header was 59.6 °C, while the average temperature of the thermocouples placed on the top header which represents the adiabatic section varied between 38.5 °C and 53.3 °C with an average of 43.8 °C. In test 2 the thermocouples on the bottom collector showed an average temperature of 63 °C while the average temperature of the thermocouples placed on the adiabatic section was 41.3 °C. The bottom header temperature in test 2 was higher than for test 1 as result of the higher temperature of the heaters.

It can be seen from the results that the water outlet temperature was fluctuating during the tests as a result of a variable thermal performance of the heat pipe which was caused by the geyser boiling occurred in the evaporator section. The average temperature of the water outlet was 13.2 °C in test 1, while it was 13.9 °C in the second test. The water inlet temperature was constant at 10.6 °C for the both tests.

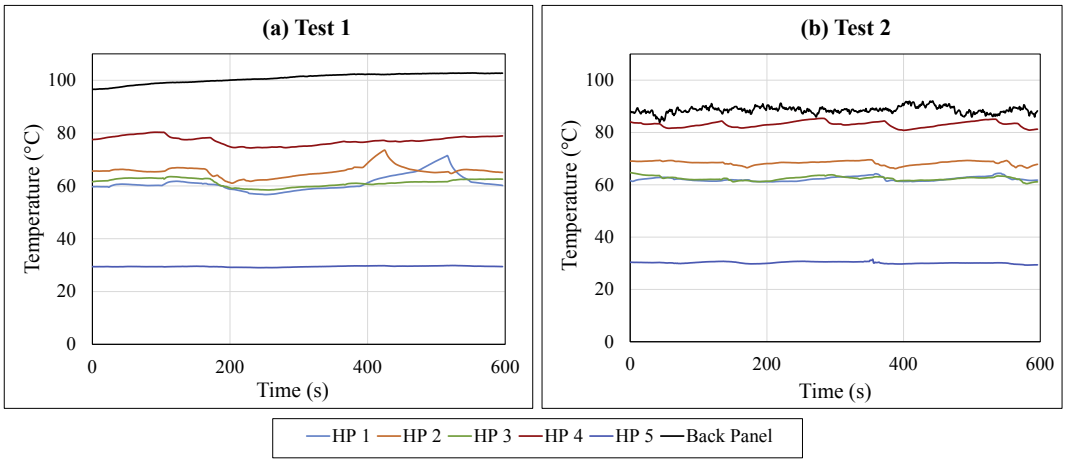

Fig. 10. FHP surface temperatures in laboratory tests 1 and 2.

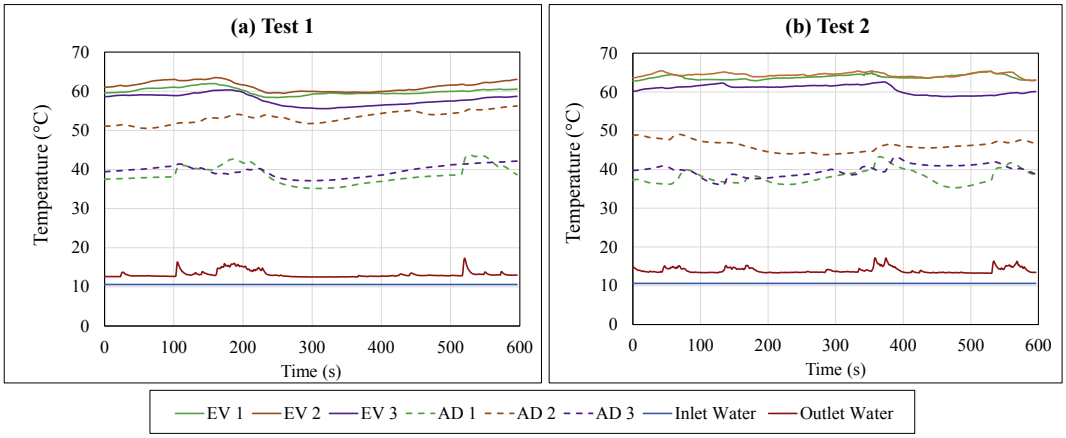

Fig. 11. FHP bottom header, adiabatic, water inlet, and water outlet temperatures during laboratory tests.

The calculated rate of heat transfer for the both experiments is illustrated in Fig. 12. In test 1, the heat transfer rate reached a maximum value of 11.4 kW and a minimum value of 2.3 kW with an average of 4.1 kW, while the heat transfer in test 2 varied between 4.3 kW and 11.5 kW with an average of 5.7 kW. The fluctuation of the results is due to the geyser boiling mentioned above. It can be observed that results in test 2 were higher than in test 1 because of the higher surface temperature of the electrical heaters. The heat transfer rate calculated for a steady state by the theoretical method for test 1 and test 2 is 4.2 kW and 6 kW, respectively. It can be seen

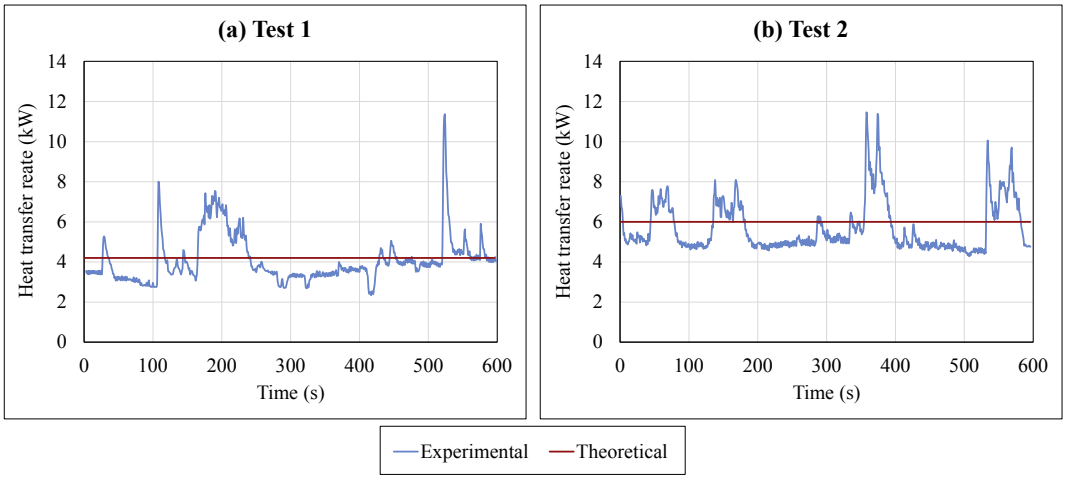

Fig. 12. The experimental and theoretical heat transfer rate of the FHP during laboratory tests.

that theoretical results were higher than the average of the experimental since the calculations do not take into account the heat loss by natural convection from the evaporator section.

5.2. Industrial test

Tests were conducted for two production processes. The first test was carried out during a high density wire production process. Fig. 13 (a) shows the temperatures of the FHP surface. The fluctuation in the data from the experiments is due to the steel production process; the steel is produced for about 120 s and then the production is paused for 40 s. It was observed that the temperature of thermocouple HP7 was the highest due to its location, the thermocouple exhibited a maximum temperature of 160 °C during the steel production process. The surface temperature of the FHP during the hot wire production varied between 111 °C and 160 °C while it decreased to the range of 84.9 °C–117.7 °C when the steel production was stopped. The back panel temperature ranged between 162 °C and 191.3 °C, as expected, higher than the temperature of the FHP surface because it was acting as fins and the thermal conductivity of the stainless steel sheet is relatively low.

The second test was performed during a low density wire production process. The heat pipe temperatures are shown in Fig. 13 (b). The surface temperatures of the Flat Heat Pipe varied between 80 °C and 51 °C. It can be observed from the results that the temperatures of the thermocouples 7, 8, 9 were higher than the temperature of the bottom collector. The film boiling present is reflected as an incremental increase as shown in thermocouple positions 4, 5, 6, 1, and 3. Thermocouple 2 had the lowest temperature value; this temperature could be explained by a false junction in the thermocouple.

The temperatures of the bottom collector and the adiabatic section of the FHP in test 1 and test 2 are presented in Fig. 14 (a) and (b). In test 1 the average temperature of the bottom collector was 66 °C at the maximum and 61 °C at the minimum when the production was stopped. The average temperature from the thermocouples placed on the top header, which represents the adiabatic section, varied between 76 °C and 66 °C. However in test 2, the thermocouples on the adiabatic section displayed temperatures of 60 °C while the three thermocouples placed on the bottom collector showed temperatures of 40 °C. It can be observed that the temperature of the bottom collector was lower than the adiabatic section because of the lack of radiative heat heating the bottom collector.

Water inlet and outlet temperatures are illustrated in Fig. 15 for both tests. The outlet temperature varied with time as a result of the variable thermal performance of the Flat Heat Pipe.

In the first test, the water inlet temperature was nearly constant at 26.2 °C while the average temperature of the water outlet was 33.4 °C. In the second test the water inlet temperature varied between 33.6 °C and 36.2 °C, while the average water outlet temperature was 41.4 °C at a maximum value of 45.3 °C.

The heat transfer rate calculated for both experiments are illustrated in Fig. 16. In test 1, the heat transfer rate varied between a maximum value of 16.9 kW and a minimum value of 9.9 kW with an average value of 12 kW. The heat transfer rate in test 2 varied between 16.1 kW and 9.2 kW with an average value of 11.6 kW. It can be observed that results in test 1 were higher than test 2 due to a higher density of steel wires. The variation in results can also be due to the location of the FHP alongside the rod conveyor. The rate of heat transfer calculated by the theoretical method was 11 kW for the both tests. It can be observed that the theoretical results less than the experimental due to the theoretical model does not take into account the heat transfer by forced convection from the hot air above the steel wires. The heat transfer rate calculated theoretically was the same for both tests since the temperature of the hot steel was the same.

The heat transfer rates of the FHP above a production line are significantly greater than during laboratory tests. This is due to a significantly higher air temperature surrounding the device in the industrial tests. The uneven surface created by the steel wires could also result in a higher effective emissivity of the heat source. If we assume that the heat recovery average of the production line is 10 kW per meter on a 70 m conveyor, the FHP will be able to recover 700 kW of wasted heat.

6. Error analysis

The main source of uncertainty for the calculated heat transfer rate values came from the temperature measurements, and the flow rate meter. The uncertainties associated these readings were detailed in Section 2.

According to [45], the propagation of uncertainties associated with the calculated heat transfer rate values (S_Q), can be calculated from:

$$S_Q = Q_{out} \times \sqrt{\left(\frac{S_{\dot{V}}}{\dot{V}}\right)^2 + \left(\frac{S_{(T_{water,out}-T_{water,in})}}{(T_{water,out}-T_{water,in})}\right)^2} \tag{25}$$

Where:

$$S_{(T_{water,out}-T_{water,in})} = \sqrt{S^2_{T_{water,out}} + S^2_{T_{water,in}}} \tag{26}$$

$$\text{The error associated with: } (T_{water,out} - T_{water,in}) \tag{27}$$

By calculating S_Q from Eq. (25)

$$S_Q = Q_{out} \times \sqrt{\left(\frac{S_{\dot{V}}}{\dot{V}}\right)^2 + \left(\frac{S_{(T_{water,out}-T_{water,in})}}{(T_{water,out}-T_{water,in})}\right)^2} \tag{28}$$

uncertainty for the maximum heat transfer rate can be listed in the table below.

The table above shows the experimental uncertainty associated with the obtained heat transfer rate values. It can be seen that the maximum error was 6.77% which is an acceptable uncertainty value.

7. Conclusions

A flat heat pipe (FHP) heat exchanger for waste heat recovery from high temperature steel production has been designed, manufactured and tested. The thermal performance of the FHP has been investigated both in laboratory and on a production line, for two different conditions. A theoretical analysis of the device has been conducted in parallel of the experimental investigation.

The rate of heat recovery during laboratory tests achieved by the FHP was about 5 kW and reasonable agreement between theory and experiment was obtained. Rather higher heat recovery was possible in the industrial tests, of the order of 10 kW, and since the device is a metre long and the production line was 70 m long, it follows that about three quarters of a Megawatt might be recovered from such an industrial plant. It can be concluded from the results that the FHP is a promising technology for waste heat recovery in the steel industry but with many challenges such as the high temperature source and limited available space on sites. More experiments should be carried out to investigate the performance of the FHP with various surface temperatures and for different inclination angles and water flow rates.

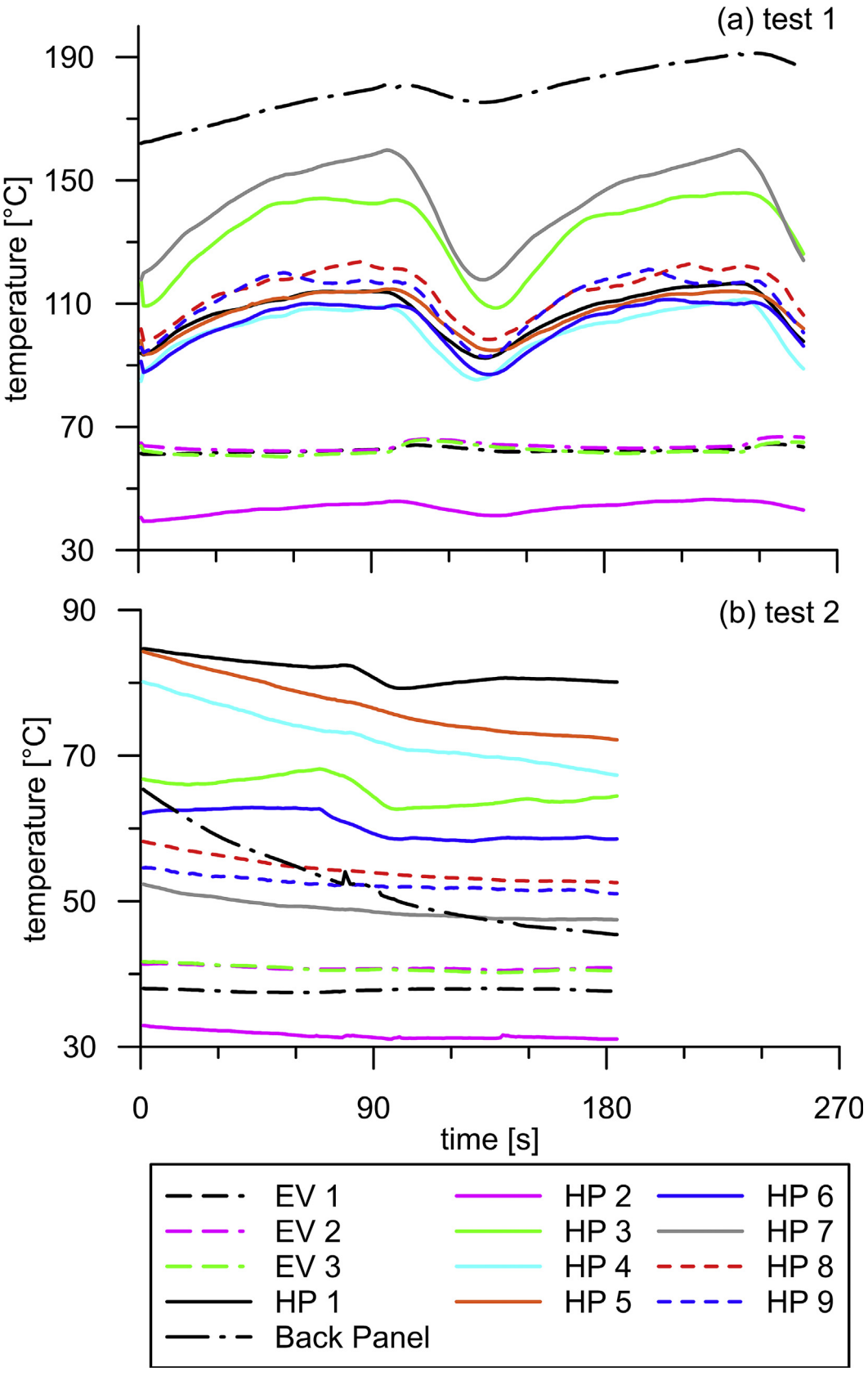

Fig. 13. Heat pipe temperatures (a) Test 1; (b) Test 2.

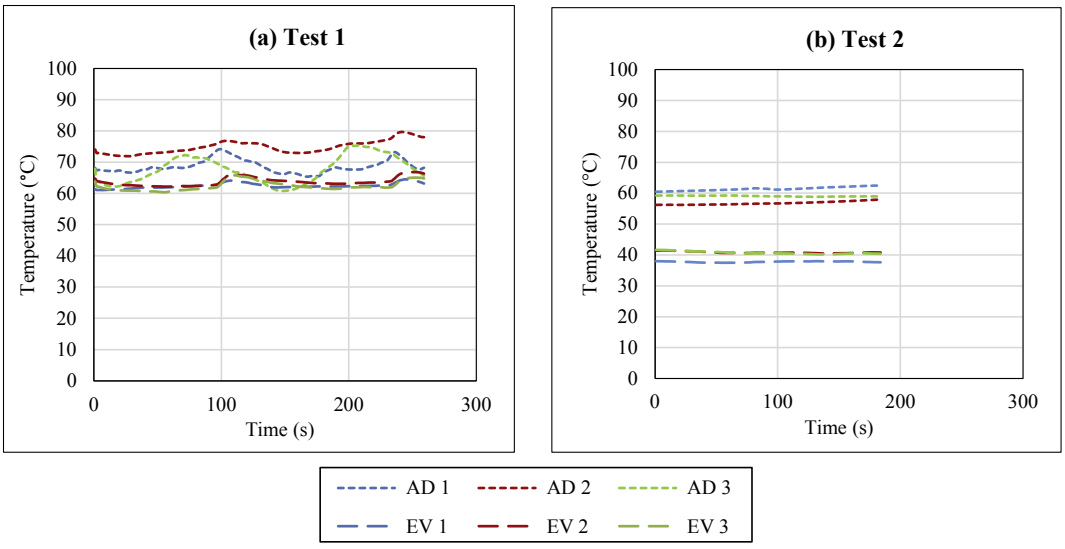

Fig. 14. Bottom collector and adiabatic temperatures of the FHP (a) Test 1; (b) Test 2.

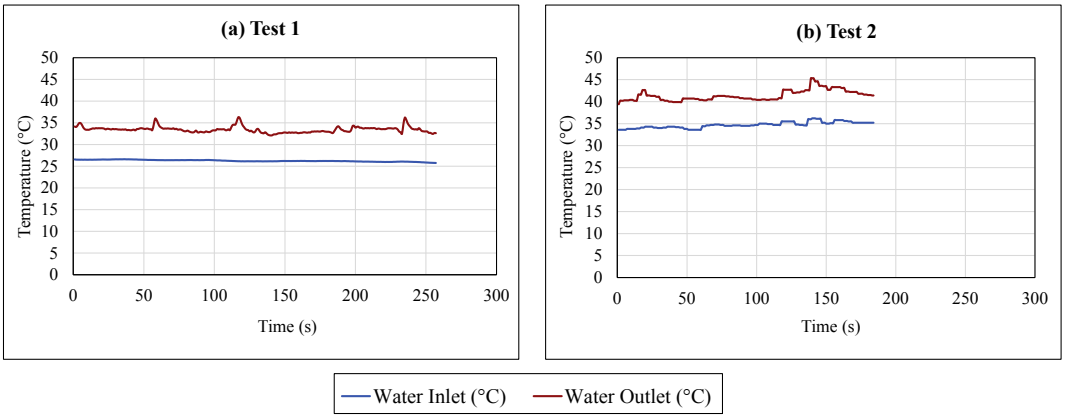

Fig. 15. Water inlet and outlet temperatures during Test 1 and Test 2.

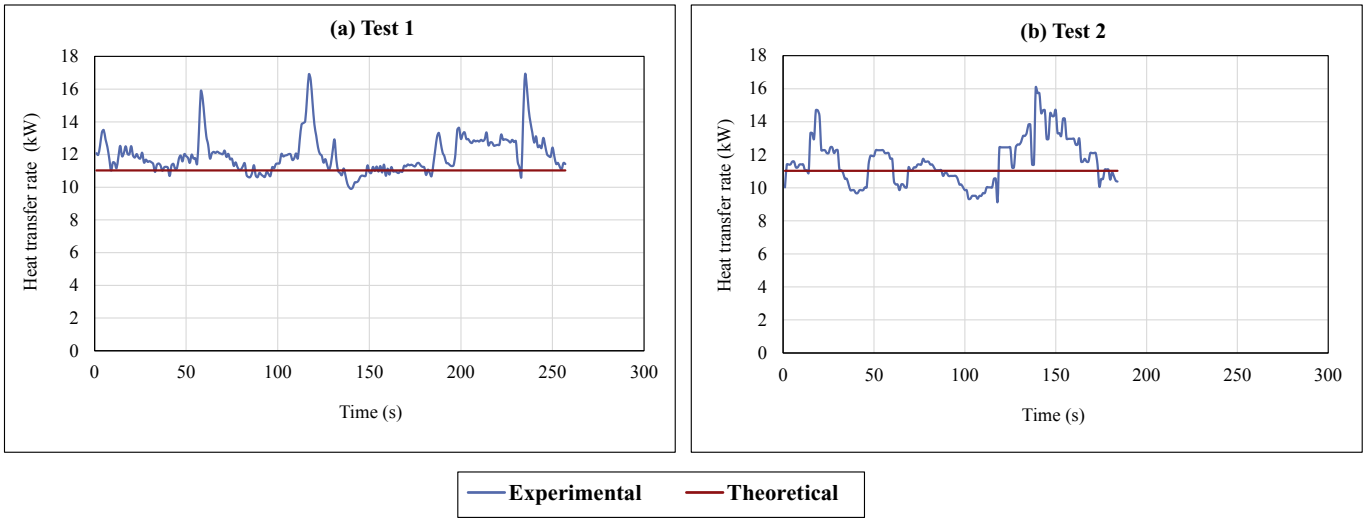

Fig. 16. Heat transfer rate: (a) Test 1 and (b) Test 2.

Acknowledgments

The research presented in this paper has received funding from the European Union's Horizon 2020 research and innovation programme under grant agreement No. 680599. The authors would like to thank Sara Diaz from Innvel Scientific Services for her technical support in the development of FHP testing carried out at a wire rod mill.

References

[1] Zhang H, Wang H, Zhu X, Qiu YJ, Li K, Chen R, et al. A review of waste heat recovery technologies towards molten slag in steel industry. Appl Energy 2013;112:956–66. https://doi.org/10.1016/j.apenergy.2013.02.019.
[2] Liu J, Yu Q, Peng J, Hu X, Duan W. Thermal energy recovery from high-temperature blast furnace slag particles. Int Commun Heat Mass Transf 2015;69:23–8. https://doi.org/10.1016/j.icheatmasstransfer.2015.10.013.
[3] Gutiérrez Trashorras AJ, Álvarez EÁ, Río González JL, Suarez Cuesta JM, Bernat JX. Design and evaluation of a heat recuperator for steel slags. Appl Therm Eng 2013;56:11–7. https://doi.org/10.1016/j.applthermaleng.2013.03.019.
[4] Kaşka Ö. Energy and exergy analysis of an organic Rankine for power generation from waste heat recovery in steel industry. Energy Convers Manag 2014;77:108–17. https://doi.org/10.1016/j.enconman.2013.09.026.
[5] Jouhara H, Anastasov V, Khamis I. Potential of heat pipe technology in nuclear seawater desalination. Desalination 2009;249:1055–61. https://doi.org/10.1016/j.desal.2009.05.019.
[6] Alammar AA, Al-Dadah RK, Mahmoud SM. Numerical investigation of effect of fill ratio and inclination angle on a thermosiphon heat pipe thermal performance. Appl Therm Eng 2016;108:1055–65. https://doi.org/10.1016/j.applthermaleng.2016.07.163.
[7] Jouhara H, Fadhl B, Wrobel LC. Three-dimensional CFD simulation of geyser boiling in a two-phase closed thermosyphon. Int J Hydrogen Energy 2016. https://doi.org/10.1016/j.ijhydene.2016.02.038.
[8] Ramos J, Chong A, Jouhara H. Experimental and numerical investigation of a cross flow air-to-water heat pipe-based heat exchanger used in waste heat recovery. Int J Heat Mass Transf 2016;102:1267–81. https://doi.org/10.1016/j.ijheatmasstransfer.2016.06.100.
[9] Jouhara H, Merchant H. Experimental investigation of a thermosyphon based heat exchanger used in energy efficient air handling units. Energy 2012;39:82–9. https://doi.org/10.1016/j.energy.2011.08.054.
[10] Jouhara H, Meskimmon R. Heat pipe based thermal management systems for energy-efficient data centres. Energy 2014;77:265–70. https://doi.org/10.1016/j.energy.2014.08.085.
[11] Ma H, Yin L, Shen X, Lu W, Sun Y, Zhang Y, et al. Experimental study on heat pipe assisted heat exchanger used for industrial waste heat recovery. Appl Energy 2016;169:177–86. https://doi.org/10.1016/j.apenergy.2016.02.012.
[12] Srimuang W, Amatachaya P. A review of the applications of heat pipe heat exchangers for heat recovery. Renew Sustain Energy Rev 2012;16:4303–15. https://doi.org/10.1016/j.rser.2012.03.030.
[13] Mathioulakis E, Belessiotis V. A new heat-pipe type solar domestic hot water system. Sol Energy 2002;72:13–20. https://doi.org/10.1016/S0038-092X(01)00088-3.
[14] Moradgholi M, Nowee SM, Abrishamchi I. Application of heat pipe in an experimental investigation on a novel photovoltaic/thermal (PV/T) system. Sol Energy 2014;107:82–8. https://doi.org/10.1016/j.solener.2014.05.018.
[15] Gang P, Huide F, Tao Z, Jie J. A numerical and experimental study on a heat pipe PV/T system. Sol Energy 2011;85:911–21. https://doi.org/10.1016/j.solener.2011.02.006.
[16] Khairnasov SM, Naumova AM. Heat pipes application to solar energy systems. Appl Sol Energy 2016;52:47–60. https://doi.org/10.3103/S0003701X16010060.
[17] Olabi AG. Energy quadrilemma and the future of renewable energy. Energy 2016;108:1–6. https://doi.org/10.1016/J.ENERGY.2016.07.145.
[18] Foley AG, Olabi Aiofe. Renewable energy technology developments, trends and policy implications that can underpin the drive for global climate change. Renew Sustain Energy Rev 2017;68:1112–4. https://doi.org/10.1016/J.RSER.2016.12.065.
[19] Tian E, He Y-L, Tao W-Q. Research on a new type waste heat recovery gravity heat pipe exchanger. Appl Energy 2017;188:586–94. https://doi.org/10.1016/j.apenergy.2016.12.029.
[20] Azad E. Interconnected heat pipe solar collector. Int J Eng Trans A Basics 2009;22:233–42.
[21] Azad E. Theoretical and experimental investigation of heat pipe solar collector. Exp Therm Fluid Sci 2008;32:1666–72. https://doi.org/10.1016/j.expthermflusci.2008.05.011.
[22] Jouhara H, Chauhan A, Nannou T, Almahmoud S, Delpech B, Wrobel LC. Heat pipe based systems - advances and applications. Energy 2017;128:729–54. https://doi.org/10.1016/j.energy.2017.04.028.
[23] Wang Y, Peterson GP. Investigation of a novel flat heat pipe. J Heat Transf 2005;127:165–70. https://doi.org/10.1115/1.1842789.
[24] Wang S, Chen J, Hu Y, Zhang W. Effect of evaporation section and condensation section length on thermal performance of flat plate heat pipe. Appl Therm Eng 2011;31:2367–73. https://doi.org/10.1016/j.applthermaleng.2011.03.037.
[25] Wang Y, Vafai K. An experimental investigation of the thermal performance of an asymmetrical flat plate heat pipe. Int J Heat Mass Transf 2000;43:2657–68. https://doi.org/10.1016/S0017-9310(99)00300-2.
[26] Tsai MC, Kang SW, Vieira De Paiva K. Experimental studies of thermal resistance in a vapor chamber heat spreader. Appl Therm Eng 2013;56:38–44. https://doi.org/10.1016/j.applthermaleng.2013.02.034.
[27] Ji X, Xu J, Abanda AM, Xue Q. A vapor chamber using extended condenser concept for ultra-high heat flux and large heater area. Int J Heat Mass Transf 2012;55:4908–13. https://doi.org/10.1016/j.ijheatmasstransfer.2012.04.018.
[28] Tang Y, Yuan D, Lu L, Wang Z. A multi-artery vapor chamber and its performance. Appl Therm Eng 2013;60:15–23. https://doi.org/10.1016/j.applthermaleng.2013.06.014.
[29] Sun Z, Qiu H. An asymmetrical vapor chamber with multiscale micro/nano-structured surfaces. Int Commun Heat Mass Transf 2014;58:40–4. https://doi.org/10.1016/j.icheatmasstransfer.2014.08.027.
[30] Wang JC. Thermal investigations on LED vapor chamber-based plates. Int Commun Heat Mass Transf 2011;38:1206–12. https://doi.org/10.1016/j.icheatmasstransfer.2011.07.002.
[31] Peng H, Li J, Ling X. Study on heat transfer performance of an aluminum flat plate heat pipe with fins in vapor chamber. Energy Convers Manag 2013;74:44–50. https://doi.org/10.1016/j.enconman.2013.05.004.
[32] Chen JS, Chou JH. Cooling performance of flat plate heat pipes with different liquid filling ratios. Int J Heat Mass Transf 2014;77:874–82. https://doi.org/10.1016/j.ijheatmasstransfer.2014.06.029.
[33] Aghvami M, Faghri A. Analysis of flat heat pipes with various heating and cooling configurations. Appl Therm Eng 2011;31:2645–55. https://doi.org/10.1016/j.applthermaleng.2011.04.034.
[34] Hou L, Quan Z, Zhao Y, Wang L, Wang G. An experimental and simulative study on a novel photovoltaic-thermal collector with micro heat pipe array (MHPA-PV/T). Energy Build 2016;124:60–9. https://doi.org/10.1016/j.enbuild.2016.03.056.
[35] Deng Y, Quan Z, Zhao Y, Wang L, Liu Z. Experimental research on the performance of household-type photovoltaic-thermal system based on micro-heat-pipe array in Beijing. Energy Convers Manag 2015;106:1039–47. https://doi.org/10.1016/j.enconman.2015.09.067.
[36] Jouhara H, Milko J, Danielewicz J, Sayegh M a, Szulgowska-Zgrzywa M, Ramos JB, et al. The performance of a novel flat heat pipe based thermal and PV/T (photovoltaic and thermal systems) solar collector that can be used as an energy-active building envelope material. Energy 2015:1–7. https://doi.org/10.1016/j.energy.2015.07.063.
[37] Wang X, Ma T, Zhu Y, Chen H, Zeng J. Experimental investigation on startup and thermal performance of a high temperature special-shaped heat pipe coupling the flat plate heat pipe and cylindrical heat pipes. Exp Therm Fluid Sci 2016;77:1–9. https://doi.org/10.1016/j.expthermflusci.2016.03.013.
[38] Yang L, Zhou RW, Ling X, Peng H. Experimental investigate on heat transfer performance of Flat Heat Pipe Receiver in Solar Power Tower Plant investigated experimentally. Compare to other traditional flat heat pipe, this heat pipe Serrated fins of solar energy at high temperature. Appl Therm Eng 2016;109:662–6. https://doi.org/10.1016/j.applthermaleng.2016.07.075.
[39] Bergman TL, Incropera FP, DeWitt DP, Lavine AS. Fundamentals of heat and mass transfer. John Wiley & Sons; 2011.
[40] Holman J. Heat transfer. McGraw-Hill Education; 2009.
[41] Rohsenow WM. A method of correlating heat transfer data for surface boiling of liquids. Cambridge, Mass: MIT Division of Industrial Corporation; 1951.
[42] Nusselt W. Die Oberflachenkondesation des Wasserdamffes the surface condensation of water. Zetrschr Ver Deutch Ing 1916;60:541–6.
[43] Rohsenow WM. Heat transfer and temperature distribution in laminar film condensation. Trans Asme 1956;78:1645–8.
[44] Gnielinski V. New equations for heat and mass-transfer in turbulent pipe and channel flow. Int Chem Eng 1976;16:359–68.
[45] Taylor J. Introduction to error analysis, the study of uncertainties in physical measurements. 1997.